Fabrication of complex hydrogel structures using suspended layer additive manufacturing (SLAM)

Senior, Jessica J.; Cooke, Megan E.; Grover, Liam M.; Smith, Alan M.

DOI:
10.1002/adfm.201904845

Document Version
Publisher's PDF, also known as Version of record

Citation for published version (Harvard):
Senior, JJ, Cooke, ME, Grover, LM & Smith, AM 2019, 'Fabrication of complex hydrogel structures using suspended layer additive manufacturing (SLAM)', *Advanced Functional Materials*, vol. 29, no. 49, 1904845. https://doi.org/10.1002/adfm.201904845

ADVANCED FUNCTIONAL MATERIALS
www.afm-journal.de

Fabrication of Complex Hydrogel Structures Using Suspended Layer Additive Manufacturing (SLAM)

Jessica J. Senior, Megan E. Cooke, Liam M. Grover, and Alan M. Smith**

There have been a number of recently reported approaches for the manufacture of complex 3D printed cell-containing hydrogels. Given the fragility of the parts during manufacturing, the most successful approaches use a supportive particulate gel bed and have enabled the production of complex gel structures previously unattainable using other 3D printing methods. The supporting gel bed provides protection to the fragile printed part during the printing process, preventing the structure from collapsing under its own weight prior to crosslinking. Despite the apparent similarity of the particulate beds, the way the particles are manufactured strongly influences how they interact with one another and the part during fabrication, with implications to the quality of the final product. Recently, the process of suspended layer additive manufacture (SLAM) is demonstrated to create a structure that recapitulated the osteochondral region by printing into an agarose particulate gel. The manufacturing process for this gel (the application of shear during gelation) produced a self-healing gel with rapid recovery of its elastic properties following disruption. Here, the physical characteristics of the supporting fluid-gel matrix used in SLAM are explored, and compared to other particulate gel supporting beds, highlighting its potential for producing complex hydrogel-based parts.

1. Introduction

The fabrication of functional tissues using extrusion-based bioprinting remains a challenge despite recent advancements in 3D (three-dimensional) bioprinting technologies. This is largely due to the complexity of tissues which are anisotropically structured down to the microscale, with local variations in biochemical and cellular composition. Bioprinting requires a bioink (material formulation including biological molecules or cells) with three key features that include compatibility with the printing technique, cytocompatible crosslinking and physicochemical similarity to that of the tissue being replicated. [1]

Biopolymer hydrogels have commonly been used to replicate tissue structures; they can be crosslinked by gentle physical interactions and have physiochemical and mechanical properties that can be tailored and controlled to resemble extracellular matrix (ECM), whilst maintaining high levels of cell viability.[2–4] Additive layer manufacture (ALM), whereby material is extruded layer-by-layer for the fabrication of 3D scaffolds, is one approach that has shown promise to enable production of cell-seeded constructs with defined geometries. Using biopolymer hydrogels as bioinks in ALM, however, remains challenging. A key issue is that the low viscosity of the hydrocolloid solutions causes them to spread when deposited onto a surface prior to gelation and sag when printing multilayered structures. This prevents the production of large, geometrically complex structures whilst maintaining shape fidelity. Moreover, tailoring and controlling variations in microstructure to replicate complex tissue within a single scaffold is difficult to achieve with these materials, as once a layer is crosslinked it is difficult to integrate the subsequent layers. To overcome these issues, high viscosity biopolymers are often used in bioinks to prevent collapse of the structure prior to gelation.[5–7] This can, however, require increased extrusion pressures to deposit the material, subsequently reducing cell viability and can also impact on cell phenotype in cells that require softer substrates. [8,9]

Embedded printing methods have been developed to overcome this limitation, where a bioink is deposited into a bath of material ranging from viscous liquids through particulate gels to solid gels with embedded phases.[10–13] These techniques enable the printing of constructs from low viscosity precursors with greater complexity and shape specificity without limitation over build direction, supports or overhangs. Despite significant efforts, these manufacturing processes have been subject to their own constraints, such as the need to enforce tight regulations on temperature control to prevent the support bed from prematurely liquefying under cell culture conditions, lack of regional mechanical variation within a single scaffold and difficulty in extracting the final product.

Suspended layer additive manufacture (SLAM) was developed in our laboratories, whereby low viscosity biopolymers

J. J. Senior, Prof. A. M. Smith
Department of Pharmacy
University of Huddersfield
Queensgate, Huddersfield, HD1 3DH, UK
E-mail: a.m.smith@hud.ac.uk
Dr. M. E. Cooke, Prof. L. M. Grover
School of Chemical Engineering
University of Birmingham
Edgbaston, B15 2TT, UK
E-mail: l.m.grover@bham.ac.uk
The ORCID identification number(s) for the author(s) of this article can be found under https://doi.org/10.1002/adfm.201904845.

DOI: 10.1002/adfm.201904845

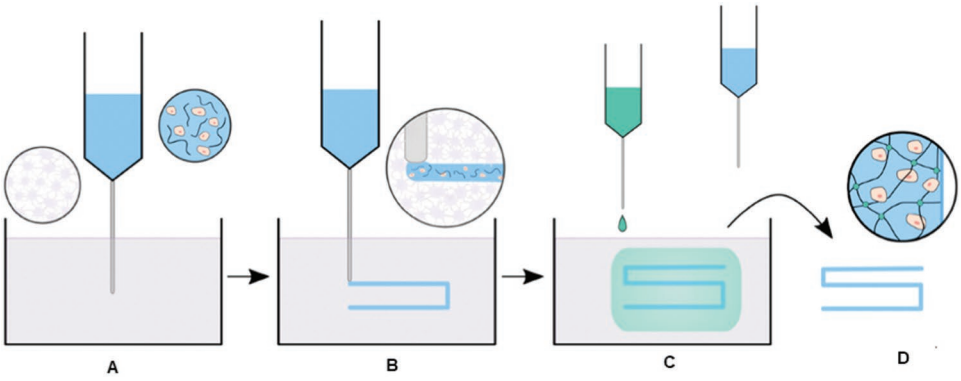

Figure 1. A schematic showing the production of a 3D bioprinted scaffold by use of SLAM. A) The fluid-gel print bed is created by shear cooling a hot agarose solution throughout the sol–gel transition which is then loaded into a container of suitable dimensions to support the scaffold. The bioinks are produced by the careful selection of hydrogel and cells and then mixing before adding to the bioprinter cartridges. B) The bioink is extruded within the self-healing fluid bed and multiple cartridges may extrude different hydrogel layers forming an interface with the pre-deposited bioinks for the creation of a multilayered construct. C) Crosslinking and cell media induces solidification and provides metabolites to the cell scaffold. D) Low shear washing with deionized water releases the construct from the supporting fluid gel.

can be extruded into a self-healing fluid-gel matrix.[14] Fluid gels are formed upon the introduction of shear during the sol–gel transition to produce a network of entangled gel microparticles, as opposed to quiescent 'bulk' gels which form markedly stronger ordered polymer networks in the absence of shear. Fluid gels exhibit solid-like behavior under low shear but liquid-like behavior when stress is applied and exhibit very fast viscoelastic recovery upon removal of stress.[15] As a result, upon extrusion of a bioink into the fluid-gel matrix, the deposited bioink is suspended in its liquid state, and collapse of the printed structure is prevented prior to gelation. This approach enables very good layer integration as no gelation is initiated during the printing process. This also allows the production of constructs from two or more different materials that have dissimilar physicochemical and mechanical properties thus creating a printed part with distinct anisotropic physical behavior. To demonstrate clinical application, we recently created a structure that recapitulated the osteochondral region (the microstructure of which changes across a hard/soft tissue interface) as directed by microcomputed tomography (micro-CT) imaging to provide accurate dimensions and was tailored to support specific cell phenotypes by controlling the microenvironment.[14] These complex scaffolds feature mechanical gradients that were similar to those found within the ECM and play a crucial role in preventing mechanical failure between interconnecting tissues as well as maintaining cell phenotype. In this study, we have further characterized the fluid-gel printing matrix and developed the SLAM technique to enable the printing of a range of composite biopolymer structures. These have then been evaluated regarding localized variations in physiochemical characteristics and cellular interaction, highlighting the potential applications of SLAM in regenerative medicine.

2. Results and Discussion

2.1. Production and Characterization of the Fluid-Gel Print Bed

Here, an agarose fluid-gel print matrix was used to enable the printing of complex geometries from low viscosity solutions (Figure S1, Supporting Information) by suspending the printed construct in its liquid form prior to gelation and extraction from the print bed (**Figure 1**). As the bioink was extruded, the fluid gel support phase acted as a liquid which underwent displacement before rapidly restructuring to support the extruded material prior to gelation (Figure 1B). When printing was complete, a crosslinker was added and allowed to diffuse through the fluid gel causing the printed construct to solidify (Figure 1C). The construct was then removed from the fluid-gel print bed and any excess fluid gel removed by gently washing with deionized water.

The structures of the agarose fluid gels were imaged using bright field microscopy (**Figure 2**A). Particles were formed of small subunits (indicated by the arrow) that interacted to form larger particles of around 100–150 µm. These 'hairy' particles were heterogeneous and irregular in shape and are generated as a result of sheared gelation as has been shown previously.[16] The formation of these hairy particles can be explained by understanding the gelation mechanism of agarose. Agarose molecules exist in a disordered random coil conformation above the gelation temperature and begin to order into helices as the temperature is reduced. When cooled further, these helices form aggregates resulting in an ordered polymer gel network. When shear is applied during this mechanism however, gel formation commences with the generation of individual gel nuclei from the disordered polymer solution as a consequence of shear forces causing disruption during molecular ordering.[17] The particles formed via this process display a high polymer density at the core of the particle with a descending gradient to the outer edge, caused by the weak intermolecular tension at the gelled and non-gelled polymer interface and the increased flow field at the particle surface. Within these lower polymer density regions at the particle surface, fewer agarose helices exist to be able to form aggregates, leading to a weaker gel and thereby deformation of the particle within the shear field to form a series of hair-like structures.[17] This is in contrast to gel particles in an agarose slurry produced by homogenization of a quiescently formed continuous gel network, which have a smooth and angular morphology (Figure 2B).

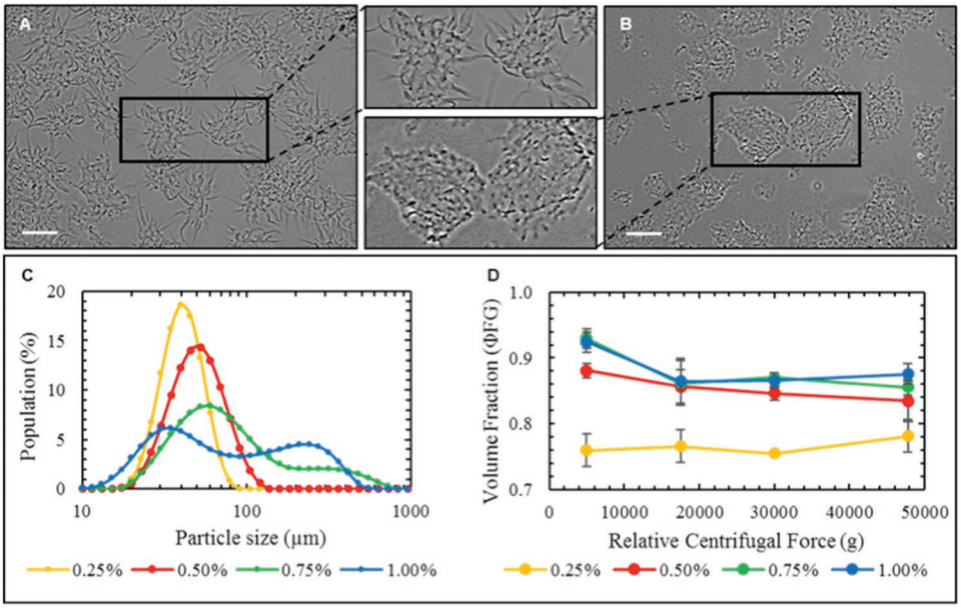

Figure 2. Assessment of the agarose fluid-gel matrix. A) Brightfield micrograph of a 0.5% w/v agarose fluid-gel-containing particles comprised of smaller subunits. B) Brightfield micrograph of a 0.5% w/v agarose slurry showing angular particles, as would be anticipated from a fractured gel, with a distinct lack of "hairy" projections (scale bars = 150 μm). C) Particle size distribution within agarose fluid gels produced at concentrations of 0.25%, 0.50%, 0.75%, and 1.00% w/v. As the concentration of agarose increases, the span of particle sizes also increases and a bimodal distribution in agarose particle size populations emerges. D) Relationship of relative centrifugal force (RCF) on solid phase volumes of fluid gels produced at concentrations of 0.25%, 0.50%, 0.75%, and 1.00% w/v. There is a significant decrease in particle fraction when the concentration of agarose is reduced from 0.50% w/v to 0.25% across all centrifugation speeds.

In order to understand the optimum fluid-gel formulation for printing, fluid gels were prepared at different concentrations of 0.25%–1.0% w/v agarose and the particle sizes and particle fractions were quantified. At concentrations above 0.5%, there was the appearance of a larger particle size population that increased with increasing concentration (Figure 2C). When printing in these higher concentration fluid gels, the greater heterogeneity in particle size causes localized areas of increased viscoelasticity which subsequently results in printed structures that are misshapen with reduced resolution. At the lower concentration, despite the particles being of a unimodal particle size, the viscosity and viscoelastic properties are much lower than at 0.5% w/v which reduces the suspending capacity of the fluid gel during printing, especially when using low viscosity biopolymers as bioink. The low viscosity and viscoelastic properties are as a result of a smaller particle fraction in the fluid gel which is known to reduce with reducing concentration.[16] To investigate this, agarose fluid gels were prepared at concentrations of 0.25%, 0.5%, 0.75%, and 1.0% w/v then subjected to a range of centrifugal forces and the mass of their solid and aqueous fractions were measured (Figure 2D). As centrifugal force increased, the fluid gels exhibited a relatively constant particle volume fraction (ΦFG) across all four centrifugation regimes. There appeared to be little difference in ΦFG between 1.0%, 0.75%, and 0.5% w/v fluid gels however, as the concentration of agarose was reduced from 0.50% to 0.25% w/v the ΦFG decreased from ≈0.85 to ≈0.75 across all centrifugation speeds. Therefore, to ensure the properties of the fluid gel are optimum for printing a uniform particle size is required with a particle size fraction > 80%.

The mechanical properties of the print bed are another critical parameter during suspended manufacture as they can impact on construct resolution and complexity. Another embedded printing technique, freeform reversible embedding of suspended hydrogels (FRESH), developed by Hinton et al., uses a gelatin slurry support bath, however the rheological behavior of such material as a suspending agent for 3D bioprinting has not been investigated in depth.[13] Here, the previously reported method for production of the gelatin slurry was replicated and the rheological properties of the two systems (gelatin slurry and agarose fluid gel) were compared with an agarose particle slurry as a control (prepared in a similar manner to the gelatin slurry). When viscosity was measured with increasing shear, to replicate the shear action of the cartridge needle within the print bed, all three formulations showed shear-thinning behavior (**Figure 3**A). This behavior is critical when employing suspended manufacture techniques, in that the movement of the needle through the gel during printing of subsequent layers does not cause dragging of the previous layers which would distort the printed construct. The agarose fluid gel exhibited lower viscosity at lower shear rates as compared with agarose or gelatin slurries, yet a more rapid, stable recovery of viscosity upon shear removal following print extrusion was demonstrated (Figure 3B,C). This first ensures that, during printing, the fluid gel can be easily displaced by the extruded bioink, yet, as importantly, undergoes fast recovery to support the suspended part. Small deformation oscillatory rheology within the linear viscoelastic region (LVR) was performed on the agarose fluid gel to determine a mechanical spectrum which revealed that it was moderately frequency dependent (Figure 3D), suggesting characteristics

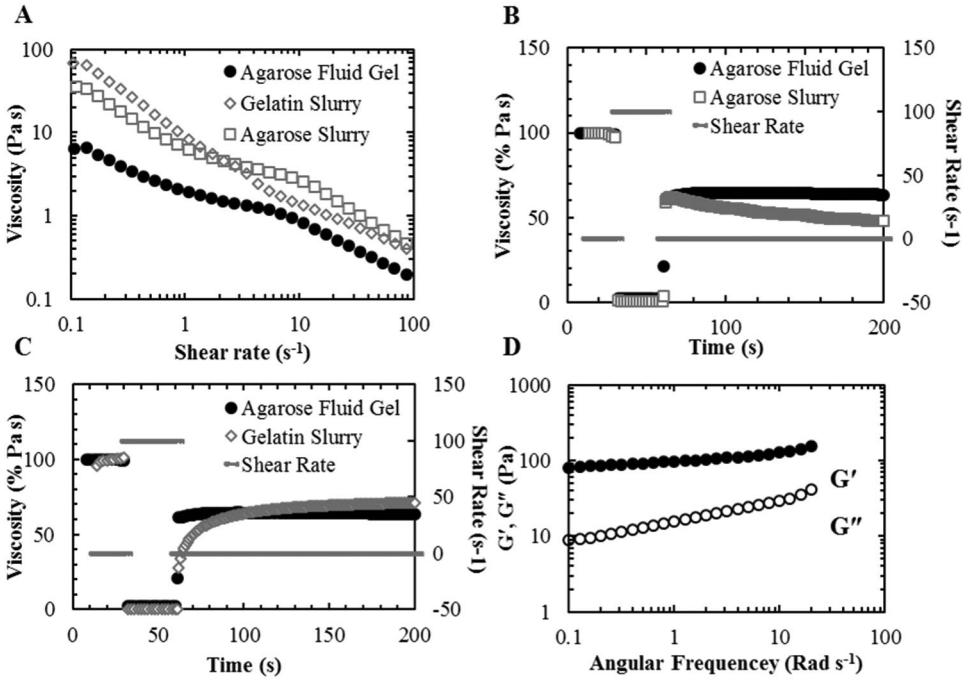

Figure 3. Mechanical spectra of the fluid-gel bed and comparison with agarose or gelatin slurry by shear rheology. A) Shear viscosity of agarose fluid gel (filled circles), gelatin slurry (blank diamonds), and agarose slurry (blank squares). Agarose fluid gels exhibit lower viscosity at lower shear rates enabling the deposition of bioinks between gelled particles. B,C) Shear recovery of agarose fluid gels versus B) agarose slurry and C) gelatin slurry. In both cases, agarose fluid gels exhibit a more rapid and stable recovery following shear removal, representing the restructuring of the gel and allowing support of the scaffold following bioink deposition within the fluid gel. D) Mechanical spectrum of a 0.5% w/v agarose fluid gel showing frequency-dependent moduli with a dominance of G' over G'' indicating the behavior of a structured fluid.

of a structured fluid with a dominance of solid (G') over liquid behavior (G'') across the frequency range tested. The contrasting mechanical behaviors of the gel slurries and the agarose fluid gel are likely a result of the different production methods that result in the core of the fluid-gel particles being more densely packed with a descending gradient to the outer edge resulting in the hair-like projections. Conversely in the FRESH system, the gelatin is quiescently gelled for 12 h before being blended resulting in a very different microstructure where the polymer concentration gradient appears to be less heterogeneous without any hairy projections. It is thought that the particle hairs of the agarose fluid gels provide a greater surface area to re-establish entanglements between particles which are responsible for the rapid viscous recovery of the material when compared to gel slurries, which have a smooth and angular microstructure.

2.2. Resolution and Diffusion of Printed Constructs

Similar to previous studies investigating bioprinting techniques, the resolution achieved in a single filament was investigated using needles of different inner diameter (or needle gauge) (**Figure 4**A–G). The potential print resolution was determined using a low viscosity dye solution. As the needle inner diameter was increased, the potential resolution decreased. Further, with larger needles, the printable filament thickness was more variable. This is likely due to both more material being extruded and also greater deformation of the fluid-gel print bed. In very low viscosity solutions of low Mw (molecular weight), diffusion is also a limiting factor for resolution (Figure 4H–J).[18] A series of lines of 1 mm width were extruded and then imaged over 2 h to investigate the rate of diffusion. As the Mw of the dye decreased, so did the time for the 2 mm gap between the printed geometry to be filled. This is important in both determining inks that can be printed using this technique and also in the rate of diffusion of crosslinking solutions that are added to the fluid-gel matrix post-printing. In other embedded techniques, such as FRESH, the gelatin slurry is formed in a calcium chloride solution such that materials that are crosslinked with divalent cations do not require the subsequent addition of crosslinking solution.[13] While this is suitable for some materials, the agarose support bath allows for further methods of crosslinking, for instance temperature-dependent polymers such as some collagen formulations are gelled by raising scaffold temperature to 37 °C which would otherwise liquefy the gelatin slurry at cell culture and physiological temperatures.

2.3. Fabrication of Complex Structures by SLAM

The bioinks used to demonstrate the variety of structures that can be produced using this technique were collagen, gellan gum, alginate, and *i*-carrageenan. These biopolymer materials have been widely investigated as tissue engineering substrates and differ in how the materials interact with cells as they have intrinsically different chemistries, gelation mechanisms, and mechanical properties. [19–22]

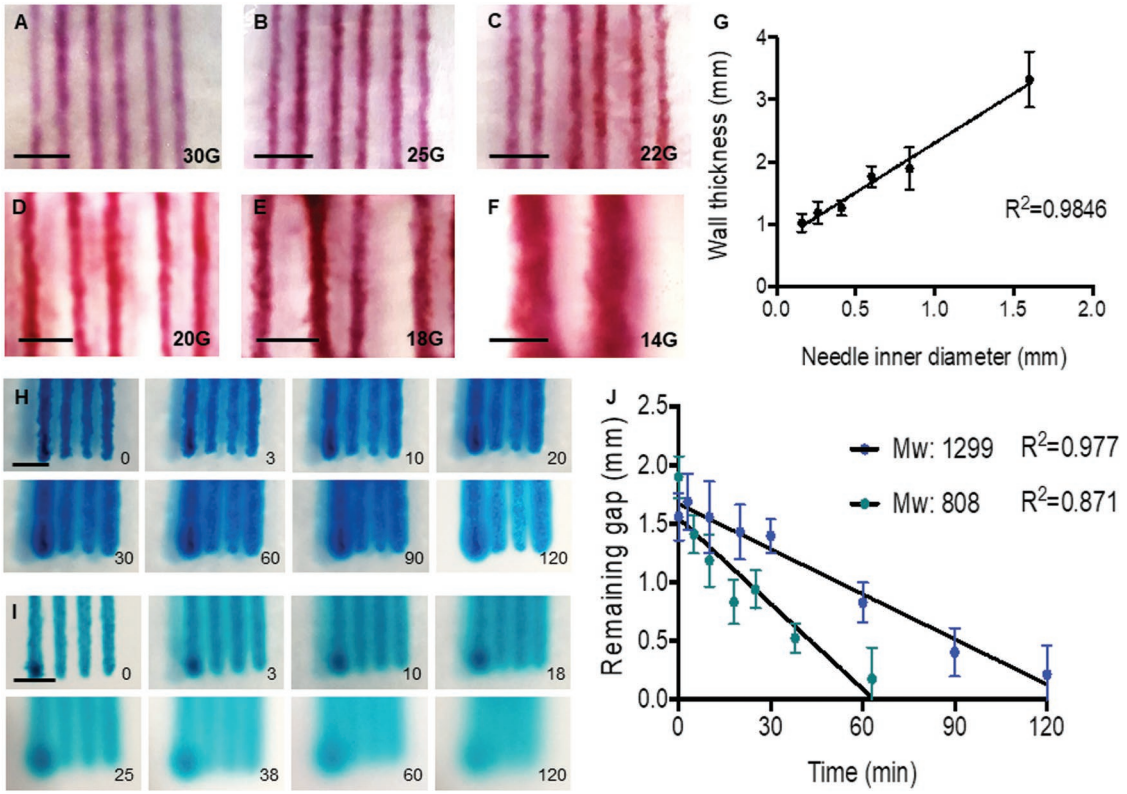

Figure 4. Optimizing print parameters within the agarose fluid gel. A–G) Resolution of bioink printed within the fluid bed support using a range of needle diameters and H–J) diffusion of dye through the fluid gel at given time points. Scale bars = 5 mm.

Different, biologically relevant geometries were printed in gellan to demonstrate the complexity and scale that can be achieved using the SLAM approach. In order to demonstrate the resolution of the system, an intricate lattice structure was printed (**Figure 5**A). The delicate structures could easily be removed from the fluid-gel bed following gelation without damage to the scaffolds. These elaborate designs are often favored in the manufacture of implantable scaffolds as they are conducive to diffusion and vascular infiltration, thus reducing the emergence of hypoxic or necrotic regions.[23–25] To display the system's capacity to print large bulk structures, a T7 intervertebral disc was manufactured (Figure 5B). The 3D printed T7 disc exhibited true-to-size dimensions and the fluid-gel print matrix successfully allowed the addition, post-production, of crosslinking cations for solidification. The ions were able to diffuse throughout the fluid gel and the whole printed part despite it having relatively large bulk dimensions ($28.0 \times 30.0 \times 6.5$ mm). The method also enabled us to produce smaller and more intricate parts as demonstrated in Figure 5C. Finally, to show the potential of producing geometries which cannot be printed using a 2D collector, a range of hollow and bifurcating structures were printed (Figure 5D,E). A large bifurcated structure ($20.45 \times 46.74 \times 22.37$) in the form of a carotid artery was printed (Figure 5D) as well as smaller, thick-walled tubular structures of 25 mm in height (Figure 5E, left and middle) and perfusable structures with internal junctions (Figure 5E, right). Following gelation, these were easily removed from the fluid-gel support bed, residual agarose was easily washed away with deionized water and they were sufficiently robust to be handled, manipulated, and perfused. These structures highlight the capability of this technique for free-form fabrication as large overhanging structures can be printed without the need for additional support structures.

Whilst the excellent work of Abdollahiet al. demonstrated the use of a carbopol supporting matrix for the fabrication of relatively complex structures from low viscosity poly(dimethylsiloxane) (PDMS) elastomer, a number of obvious implications still remain.[26] First of all, some 3D prints were unable to retain structural integrity following retrieval from the supporting Carbopol matrix and thus required suspension in water, whilst other, bifurcated structures required additional mechanical reinforcements using a webbed fork. These issues pose a problem regarding the suitability of printed constructs in tissue engineering and research contexts, with scaffold handleability and the manufacture of scaffolds with distinct dimensions, without the need for additional supports, being compromised. Additionally, in order to integrate multiple layers using these materials, pressure is required to aid the fusion of layers below, rendering this technique incapable of achieving lateral fusion and limiting the print orientation within the system. Using the SLAM method however, deposition of multiple layers has been demonstrated horizontally, laterally and also within a previously deposited extrude[14,15] thus enabling the production of constructs with biochemical and mechanical gradients as exhibited in native tissues. Another limitation with the freeform reversible embedding method is

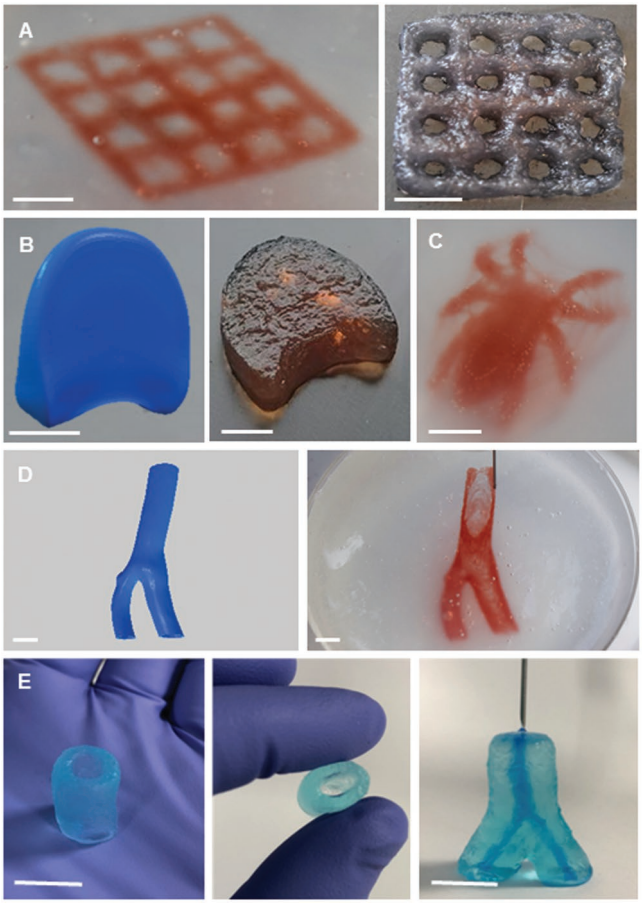

Figure 5. Fabrication of complex structures by SLAM using gellan. A) Intricate lattice prior to (left) and following extraction (right) from the fluid-gel bed. B) T7 intervertebral disc as a CAD file (left) and demonstrating the printing of bulk structures with lateral (middle) and apical (right) views. C) Intricate bulk structure in the form of a gellan spider. D) Carotid artery as a CAD file (left) and during 3D printing (right). D) Tubular structure (left) demonstrating material durability (middle) and perfusibility. Scale bars = 10 mm.

that curing of PDMS is implemented either at 65 °C for 4 h or at room temperature for 72 h. In both cases, these conditions are not conducive to the introduction of cells within the system. Curing scaffolds for shorter periods requires excessive temperatures that are unfavorable for cell culture, causing apoptosis and necrosis. Alternatively, scaffolds cured over longer time periods would subject cells to more ambient temperatures, yet the introduction of cell culture media into the system, which is crucial for cell metabolism whilst curing, would liquefy the carbopol support due to the presence of monovalent cations. This would subsequently cause premature release and distortion of the structure prior to fully curing.

Likewise, although Hinton et al. have intelligently devised an algorithm in order to address the issues associated with print resolution and fidelity, the problems relating to incorporation of cells within PDMS scaffolds have still been disregarded.[27] In cases where defective tissues exhibit compromised cellular mitotic activity, intervention through the incorporation of exogenous cells within biofabricated constructs is pertinent.

Microextrusion was the method of choice for incorporation into process that is reported in this paper. It allows for continuous dispensing of bioinks rather than deposition through droplet formation as conducted in inkjet printing, leading to improved dispensing precision. Microextrusion printing also offers greater freedom with regards to cell densities within the bioink.[28] Previous studies have indicated that the use of inkjet printers enables a reduction in print-induced shear stresses applied to suspended cell populations compared with microextrusion methods, however, there are key features of the supporting bed utilized for SLAM that enable shear minimization utilizing microextrusion.[29] The key parameters that cause shear induction in bioinks are: printing pressure; material viscosity; and dispensing nozzle diameter. These parameters also dictate print resolution and thus careful consideration must be taken in designing a process to maximize both resolution and cell viability. The main advantage of using a supporting fluid-gel bed in SLAM is that it allows for the use of low viscosity bioinks—indeed we have demonstrated that the supporting bed will geometrically localize water stained with a low molecular weight dye for a significant period of time. The capacity to print with such low viscosity materials reduces the need for high print pressures during the printing process meaning that shear forces to which cells are exposed are reduced compared to other microextrusion-based systems. In comparison with the inkjet system used by Paxton et al., who detailed how their methods imparted low shear stresses on cells, we were able to obtain 3D printed structures using lower print pressures (0.01 –0.26 bar versus 1–5 bar), lower bioink viscosities and a larger range of needle diameters (159–1600 µm versus 125–165 µm).[30] Using our system, it has therefore been demonstrated that the issues associated with cell shearing during microextrusion can be easily reduced, achieving admirably low shear stresses on cells that rival those seen during other forms of biofabrication including drop-on-demand techniques such as inkjet printing.

2.4. 3D Printing Multilayer Gradient Scaffolds by SLAM

To achieve the overall aim of reproducing functional tissue, multiple materials are required to satisfy the mechanical, chemical, and biological variations that occur throughout native tissue. Control of spatial deposition of cells within a specific material is one of the key advantages of 3D bioprinting, however, the incorporation of multiple materials interfaced into a single structure is particularly challenging when using biopolymer hydrogels. This problem can relatively easily be overcome by using the SLAM approach. We have recently demonstrated this by producing an osteochondral construct where ex vivo chondrocytes were deposited into a layer of gellan gum and osteoblasts were deposited into a gellan-hydroxyapatite layer guided by a micro-CT image of an osteochondral defect.[14] We have now further developed the concept by printing integrated structures that have different gelation mechanisms and significantly different chemistries. Ionotropically gelled (alginate, gellan, and ι-carrageenan) and thermally gelled (collagen) biopolymers were successfully integrated to form interfacing, dual-phase scaffolds (Figure 6A,B,

and Figure S2, Supporting Information). The adjacent materials interact with one another to a sufficient extent that (Figure S3, Supporting Information) mechanical failure does not occur as a clean break between the neighboring layers. Scanning electron microscopy (SEM) demonstrated the intimate interface between the hydrogel phases, and staining of sections demonstrating colocalization of the different materials (Figure S3, Supporting Information). Although this is not evidence of molecular level interpenetration, it is clear that the materials blended to the extent that mechanical failure does not occur between the materials. Composite structures such as these more closely mimic native tissue environments as they emulate the graduated mechanical and chemical constituents of which tissues are comprised. Furthermore, this technique of printing integrated layered structures is not only compliant to printing different materials layer upon layer, but also deposition of a second material into the center of another. For example, in addition to producing layered constructs, it was possible to create 3D printed core–shell structures comprising a cylindrical core of collagen encapsulated within a gellan or alginate cylinder with various dimensions (**Figure 6**C,D). Core–shell scaffolds are utilized within a number of applications including the delivery of single or multiple therapeutic drugs and bioactive molecules, loading scaffolds as cell carriers and also for the preservation of potent stem cell characteristics.[31,32] Their intelligent design allows for compartmentalization of these biological agents for tissue regeneration, where the shell generally protects the inner core and controls the release of its suspended contents. Controlled spatial deposition of these materials and their biological cargo by SLAM therefore offers a multitude of possibilities for novel therapeutic interventions. Another advantage of being able to deposit scaffold material precisely is that cell behavior can be spatially manipulated. Polymers such as collagens that are saturated with integrin binding domains allow cell attachment to the scaffold, whereas alginate and gellan do not naturally possess cell attachment motifs and instead, encapsulate cells with minimum attachment to the surrounding material (Figure 6E).[4,33] Further, collagen and alginate are dissimilar with regards to porosity and microarchitecture which can also impact on cell behavior. Collagen/alginate bilayer scaffolds were lyophilized and imaged using micro-CT in order to outline the microarchitectural differences between the adjoining layers (Figure 6F). These scaffolds exhibited an overall average porosity of 88.22% which is more than adequate for cell traction and motility, metabolite diffusion within the scaffold and for the penetration of vasculature.[25] Distinct gradients in porosity could also be visualized with an identifiable interfacial region where pore size gradually changes. Having porosity gradients can be particularly useful in allowing specific cell types to migrate during tissue regeneration and to facilitate mechanical interlocking between the scaffold and biological tissue in vivo, thus enhancing mechanical stability.[25] It was then demonstrated that both cell adhesive (collagen) and cell non-adhesive (alginate) materials could be loaded with human dermal fibroblasts (HDFs) within a singular structure (Figure 6G). The way in which the cells interacted with the materials following culture over 5 d showed distinct regional variation. It was clear that HDFs in the collagen layer had attached, having an extended morphology. Within the alginate layer (which lacks cell attachment motifs)

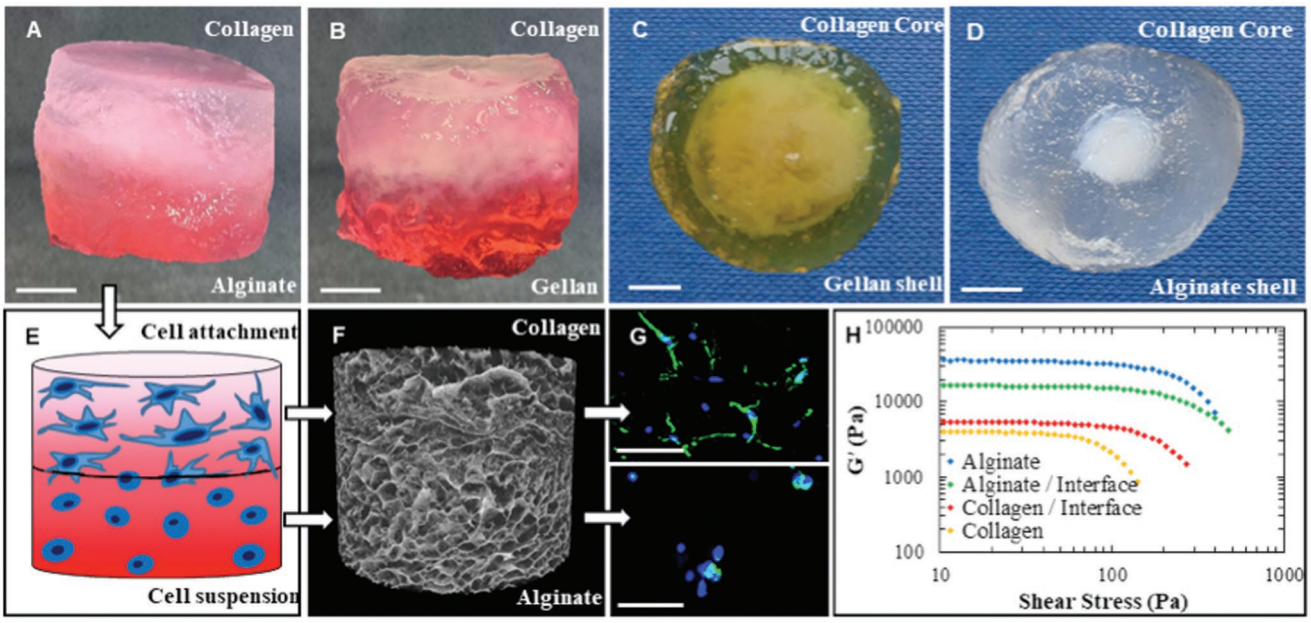

Figure 6. 3D printing multilayer gradient scaffolds by SLAM. A,B) Images of bilayer scaffolds using combinations of A) collagen-alginate and B) collagen-gellan. C) Large collagen-core gellan-shell scaffold and D) small collagen-core alginate-shell scaffold (scale bars = 5 mm). E) Schematic of diagram showing control of cell behavior with attachment motif bearing complexes in the upper collagen gel and no attachment motifs for cell suspension within an alginate gel. F) Micro-CT showing gradient porosity within a lyophilized collagen-alginate scaffold. G) Confocal micrographs of Hoechst/actin cell staining of HDFs attached in the collagen layer (upper) and suspended in the alginate (lower) regions of a dual layer scaffold (scale bars = 100 µm). H) Stress versus G' showing variations in gel strength and elasticity across a collagen-alginate scaffold including the interfacial regions illustrating a gradient in mechanical strength across the printed part.

the cells assumed a spherical morphology. This demonstrates how cell–material interactions can be controlled within a single structure by using hydrogels containing differing chemical constituents. While scaffolds bearing integrin binding domains allow migration of cells throughout the scaffold (as well as the infiltration of endogenous cells from the site of implantation), alternatively, suspending cells may be more advantageous for scaffolds that are destined for long term implantation. By encapsulating cells, they can be (reversibly) mitotically and metabolically inhibited, preventing overproliferation within the scaffold and giving the implant optimal time to become vascularized as has previously been reported.[34] The entrapped cells may then be released during scaffold degradation and the cell cycle is resumed. Essentially, the selection of the material to be used in implantable scaffolds is highly dependent on the intent of the scaffold itself, though materials are generally selected on the basis that their rate of degradation matches new tissue formation.[35]

Another way in which cells may be manipulated by tailoring the scaffold microenvironment is in the design of construct mechanics. Cells are capable of responding to external mechanical stimuli via mechanotransduction processes and will respond appropriately to such stimulation through mechanoreciprocity. The variety of mechanical stimuli they experience include hydrostatic pressure, shear, compression, and tensile force that is generated locally within discrete tissues by cell–cell or cell–ECM interactions.[36] Therefore, the behavior of cells is tissue-specific. Within mechanically static or compliant tissues such as within neural tissues, stiffnesses are relatively low ($\approx 5 \times 10^1$ Pa). In contrast, tissues exposed to high mechanical loading, such as bone or skeletal muscle, exhibit ECM stiffness that is several orders of magnitude greater ($\approx 2–4 \times 10^9$ Pa).[37] To determine differences in mechanical behavior throughout the bilayered structures, rheological measurements of viscoelasticity were performed on the various regions of the structures. Amplitude stress sweeps of alginate/collagen constructs revealed large regional variations in viscoelastic behavior. Storage moduli (G') of 4107, 5471, 16 570, and 37 170 Pa were measured at a shear stress of 10 Pa for the collagen, collagen/interface, gellan/interface, and gellan regions, respectively (Figure 6H). The LVR (and therefore the critical stress at which intermolecular associations are forced to collapse) also showed a reduction in a graduated manner throughout the whole of the hydrogel scaffolds. By matching the mechanical properties of tissue engineering scaffolds to those of the desired tissue by controlling factors such as polymer chemistry, concentration, and porosity, it is possible to mimic a range of native tissues using SLAM. Another platform which could potentially benefit from the SLAM technique, other than implantation for regenerative purposes, is the production of scaffolds for drug-disease modeling. For example, during pathogenesis and the development of cancerous tissues within the breast, tissue stiffness can increase as much as tenfold than that of healthy breast tissue.[38] This system therefore holds the potential to create healthy transplantable tissues that mimic transplant destinations in vivo and to recreate model drug-disease environments in vitro in a bid to combat degenerative diseases using SLAM.

3. Conclusion

In summary, we have demonstrated that the SLAM technique can be used to overcome the problems associated with using low viscosity bioinks in extrusion-based bioprinting. The method enabled the successful fabrication of bulk, intricate, dual phase, and phase-encapsulated hydrogels from a variety of biopolymer materials that are currently widely investigated in regenerative medicine. Furthermore, it was shown that controlled spatial gradients in mechanical and chemical properties can be produced throughout a single part with interface integrity between different materials. This allows for physicochemical properties of the structure to be designed accordingly with the ability to control porosity, mechanical gradients, cell distribution, and morphology. Our findings suggest many different tissue types could be replicated using SLAM by carefully selecting and designing bioinks to dictate cellular fate and phenotype. Overall, SLAM is a promising technique for producing delicate soft tissues, complex soft tissue structures, and interfaced tissues.

4. Experimental Section

Fluid-Gel Preparation: For formulation of the print bed, agarose fluid gels were prepared by cooling autoclaved agarose (type 1 low EEO, purchased from Sigma–Aldrich, UK) dispersed in deionized water at 0.5% w/v concentration to 25 °C under a constant shear of 700 rpm. Fluid gels were then loaded into extra-depth tissue culture plates.

Hydrogel Slurry Preparation: Gelatin and agarose slurries were produced as the FRESH method.[13] Briefly, a 4.5% w/v gelatin solution was produced in 11×10^{-9} M $CaCl_2$ (0.5% w/v agarose in dH_2O) and gelled overnight at 4 °C. 350 mL 11×10^{-9} M $CaCl_2$ (dH_2O for agarose) was added and pulsed intermittently for 120 s in a blender. The slurries were then centrifuged at 4200 rpm for 2 min before the supernatant was removed. $CaCl_2$ (or dH_2O) was added before centrifuging again (removing uncrosslinked polymer); the supernatant was removed and slurries were stored at 4 °C prior to analysis.

Preparation of Polymer Solutions for Printing: The materials used for printing were low acyl gellan gum and ι-carrageenan (purchased from Special Ingredients, UK). Powders were dispersed in deionized water at concentrations of 1.0% and 2.0% w/v, respectively, and allowed to cool from 85 °C to 25 °C to form working solutions. Alginate (alginic acid sodium salt, purchased from Sigma–Aldrich, UK) solutions were prepared at 3.0% w/v concentration similarly to gellan gum and ι-carrageenan and 0.5% w/v PureCol EZ Gel collagen solutions (Advanced BioMatrix, purchased from Sigma–Aldrich, UK) were stored at 4 °C prior to use.

Optical Microscopy: For visualization of the particulate structure within fluid gels, small samples were loaded onto microscope slides and mounted with a cover slip before imaging using a VWR IT 400 Inverted Microscope (VWR, UK).

Fluid-Gel Particle Size Distribution: Particle size distribution within the fluid gels was examined using a Malvern Mastersizer 2000. Fluid-gel samples of 0.25%, 0.50%, 0.75%, and 1.00% w/v were shear cooled under 700 rpm and diluted in deionized water followed by agitation at 2450 rpm in order to give a homogenous dispersion of particles prior to particle sizing analysis. Data from an average of 10 replicates were used. A refractive index of 1.42 and 1.33 was used for agarose and deionized water, respectively.

Fluid-Gel Particle Volume Fraction: For the determination of fluid-gel particle volume fractions, agarose fluid-gel samples at concentrations of 0.25%, 0.50%, 0.75%, and 1.00% w/v were centrifuged at a given range of centrifugal forces (RC5C Sorvall Instruments-Dupont, Wilmington, DE) in order to retrieve fluid-gel particles from the continuous aqueous

phase. The solid phase volume of the fluid gel following centrifugation (ΦFG) was then calculated as a fraction of the mass of sedimented solid (MFG.s) compared with the total pre-centrifuged fluid gel (MFG.0) as displayed in Equation (1.1).

$$\varphi\mathrm{FG} = \frac{\mathrm{MFG.s}}{\mathrm{MFG.0}} \tag{1.1}$$

In order to account for the fluid released from the particles themselves during the centrifugation process, quiescent agarose bulk gels of identical concentrations were also centrifuged. The solid phase volume of the quiescent bulk gel following centrifugation (φQG) was then calculated as a ratio of the mass of sedimented solid (MQG.s) compared with the total pre-centrifuged quiescent bulk gel (MQG.0) as reported in Equation (1.2).

$$\varphi\mathrm{QG} = \frac{\mathrm{MQG.s}}{\mathrm{MQG.0}} \tag{1.2}$$

The fluid expelled from fluid-gel particles due to particle compressibility can therefore be expressed as $1 - \varphi QG$.

Finally, a third contributor to liquid expulsion can be attributed to gel relaxation—also known as syneresis (φsyn). This was quantified as the mass of the fluid released from quiescent gels following a 72-h period divided by the total original mass of quiescent bulk gels for given concentrations.

The fluid-gel particle volume fraction for a given polymer concentration and centrifugal force may then be ascertained according to Equation (1.3).

$$\Phi\mathrm{FG} = \varphi\mathrm{FG} + \left[\left(1 - \varphi\mathrm{QG}\right) - \varphi\mathrm{syn}\right] \tag{1.3}$$

Lyophilization: Collagen-core alginate-shell scaffolds were cross-sectioned and placed in −80 °C conditions for 24 h and then a 72 h freeze drying cycle was implemented at −76 °C and 0.0010 mbar (Christ ALPHA 2–4 LD plus). Dry samples were stored in a desiccator prior to imaging.

Scanning Electron Microscopy: Lyophilized collagen-core alginate-shell scaffolds were prepared for SEM by sputter coating with gold using a Quorum SC7620 sputter coater under a low bleed of argon. The internal networks within the samples were then studied using a field emission SEM (FEI Quanta 250 SEM) operated in high vacuum mode at an accelerated electron energy of 20 kV. Images were collected using a backscattered electron detector.

Rheological Testing for the Comparison of Print Beds: Rheological analyses of the agarose fluid gel, gelatin slurry, and agarose slurry were performed in triplicate at 25 °C using a Kinexus Ultra+ rheometer (Malvern Panalytical, UK). Stress sweeps were performed at 1 rad s^{-1} between 0.1–50 Pa to determine the LVR, frequency sweeps were then performed at 0.25% strain between 0.1–50 rad s^{-1}. To investigate the shear thinning behavior, the shear rate was ramped from 0.1 to 100 s^{-1}. Finally, three-step thixotropic measurements were performed at 0.1–100–0.1 s^{-1}.

Design of Scaffolds: 3D lattice and dual layer scaffolds were designed using computer-aided design (CAD) software SolidWorks and saved in stl (stereolithography) file format, which describes the 3D model in a surface tessellated arrangement. T7 intervertebral discs, spider and carotid artery designs were downloaded from thingiverse (https://www.thingiverse.com/). The stl to G-code conversion programme Slic3r was then used to slice the models into layers and translate the coordinates into commands for the 3D bioprinter.

Fabrication of 3D Printed Scaffolds: For the printing of 3D structures by suspended manufacture, bioink cartridges were loaded with hydrogel (gellan, collagen ι-carrageenan, or alginate), attached to a conical nozzle with an internal diameter (ID) of 410 µm and inserted into an INKREDIBLE 3D bioprinter (Cellink, Sweden). In some cases, phenol red or red/blue food dye was added to the hydrogels for improved visualization of the scaffolds. The 3D bioprinter was calibrated to a specified pressure followed by placement of the petri dish containing the agarose fluid bed upon the *z*-stage. For the fabrication of multilayer hydrogel scaffolds, an additional cylinder was printed directly above the previously extruded cylinder, prior to gelation, allowing integration between the two layers. For core–shell scaffolds, a collagen cylinder was printed within a pre-printed gellan or alginate cylinder. Gellan gum, ι-carrageenan and alginate were ionically crosslinked with the extrusion of 200×10^{-9} M of $CaCl_2 \cdot 2H_2O$ around the structure through a hypodermic needle, whereas collagen gelation was induced thermally by raising the temperature to 37 °C. Finally, the constructs were retrieved from the agarose bed using a spatula and a low shear wash was applied with deionized water.

Micro-Computed Tomography: In order to assess the microstructure and porosity of dual phase sponges, alginate-collagen, and gellan-collagen samples were imaged using micro-CT with the following parameters: no filter, 30 kV, 70 µA, pixel size 6.76 µm, 1000 ms exposure, 0.3° rotation step, four-frame averaging (Bruker Skyscan 1172, Bruker, Belgium) and reconstructed data were visualized in 3D using CTVox software (Bruker).

Cell Seeding and Morphology: HDFs were cultured to passage 3 before being seeded at 1×10^6 cells mL^{-1} into either medium viscosity alginate (Sigma–Aldrich) or PureCol EZ gel (Sigma–Aldrich). They were then printed sequentially to produce bilayered constructs using a modified Duplicator i3 (Wanhao). Following 3 d culture, cell morphology was assessed by actin and Hoechst staining (Invitrogen).

Rheological Testing on Dual Layer Scaffolds: All rheological testing on 3D-printed scaffolds was undertaken in triplicate using a Bohlin Gemini rheometer (Malvern Panalytical, UK) with a 20 mm parallel plate geometry and a lower serrated plate at 25 °C. Construct regions were sectioned to 1 mm thickness prior to evaluation using a surgical scalpel. Stress sweeps were carried out to compare and characterize the differences in the LVR and stress at failure within the varying regions of dual phase scaffolds. Elastic (G') and viscous (G'') moduli (Pa) were measured with increasing shear stress from 1 to 1000 Pa at a constant angular frequency of 10 rad s^{-1}.

Profilometry: Polymer interface and surface texture of dual layer freeze-dried scaffolds were examined using Talysurf CCI 3000 optical 3D surface profiler. Scaffolds were placed in −80 °C conditions for 24 h and then a 72 h freeze drying cycle was implemented at −76 °C and 0.0010 mbar (Christ ALPHA 2–4 LD plus). Dry samples were stored in a desiccator prior to imaging. Freeze dried cylindrical dual layer scaffolds (25×10 mm) were affixed onto a stainless steel wafer (30×30 mm) and then placed under the microscopic arm of the profiler. 800×800 µm regions of the scaffolds were scanned to obtain reliable statistics. The height variation in the resulting topography maps was represented by a color scheme from which the topographical information could be reliably inferred. Surface roughness was determined using Surfstand Software.

Supporting Information

Supporting Information is available from the Wiley Online Library or from the author.

Acknowledgements

J.J.S. and M.E.C. contributed equally to this work. The authors would like to thank Dr. Muhammad Usman Ghori for his assistance with the profilometry measurements (Figure S3, Supporting Information). In addition, the authors would like to acknowledge the Doctoral Training Alliance Applied Biosciences for Health and the University of Huddersfield for provision of a studentship (J.S.), and the EPSRC for the provision of a studentship (M.E.C.) through the Sci-Phy-4-Health Centre for Doctoral Training (EP/L016346/1).

Conflict of Interest

The authors declare no conflict of interest.

Keywords

additive layer manufacture, biomaterial, biopolymer, bioprinting, hydrogel, tissue engineering

Received: June 17, 2019
Revised: August 22, 2019
Published online: September 27, 2019

[1] J. Malda, J. Visser, F. P. Melchels, T. Jüngst, W. E. Hennink, W. J. A. Dhert, J. Groll, D. W. Hutmacher, *Adv. Mater.* **2013**, *25*, 5011.
[2] W. Hu, Y. Xiao, S. Zhang, J. Wang, Z. Wang, *Biomater. Sci.* **2019**, *7*, 843.
[3] H. Geckil, F. Xu, X. Zhang, S. Moon, U. Demirci, *Nanomedicine* **2010**, *5*, 469.
[4] M. W. Tibbitt, K. S. Anseth, *Biotechnol. Bioeng.* **2009**, *103*, 655.
[5] Y. He, F. Yang, H. Zhao, Q. Gao, B. Xia, J. Fu, *Sci. Rep.* **2016**, *6*, 29977.
[6] T. Boland, X. Tao, B. J. Damon, B. Manley, P. Kesari, S. Jalota, S. Bhaduri, *Mater. Sci. Eng. C* **2007**, *27*, 372.
[7] B. Duan, L. A. Hockaday, K. H. Kang, J. T. Butcher, *J. Biomed. Mater. Res., Part A* **2013**, *101A*, 1255.
[8] K. Fakhruddin, M. S. A. Hamzah, S. I. A. Razak, *IOP Conf. Ser.: Mater. Sci. Eng.* **2018**, *440*, 12042.
[9] R. G. Wells, *Hepatology* **2008**, *47*, 1394.
[10] D. F. Duarte Campos, A. Blaeser, M. Weber, J. Jäkel, S. Neuss, W. Jahnen-Dechent, H. Fischer, *Biofabrication* **2013**, *5*, e015003.
[11] C. B. Highley, C. B. Rodell, J. A. Burdick, *Adv. Mater.* **2015**, *27*, 5075.
[12] T. Bhattacharjee, S. M. Zehnder, K. G. Rowe, S. Jain, R. M. Nixon, W. G. Sawyer, T. E. Angelini, *Sci. Adv.* **2015**, *1*, e1500655.
[13] T. J. Hinton, Q. Jallerat, R. N. Palchesko, J. H. Park, M. S. Grodzicki, H. J. Shue, M. H. Ramadan, A. R. Hudson, A. W. Feinberg, *Sci. Adv.* **2015**, *1*, e1500758.
[14] S. R. Moxon, M. E. Cooke, S. C. Cox, M. Snow, L. Jeys, S. W. Jones, A. M. Smith, L. M. Grover, *Adv. Mater.* **2017**, *29*, e1605594.
[15] M. E. Cooke, S. W. Jones, B. ter Horst, N. Moiemen, M. Snow, G. Chouhan, L. J. Hill, M. Esmaeli, R. J. A. Moakes, J. Holton, R. Nandra, R. L. Williams, A. M. Smith, L. M. Grover, *Adv. Mater.* **2018**, *30*, e1705013.
[16] I. T. Norton, D. A. Jarvis, T. J. Foster, *Int. J. Biol. Macromol.* **1999**, *26*, 255.
[17] I. Fernández Farrés, R. J. A. Moakes, I. T. Norton, *Food Hydrocolloids.* **2014**, *42*, 362.
[18] A. H. P. Skelland, X. Meng, *Polym.—Plast. Technol. Eng.* **1996**, *35*, 935.
[19] L. Cen, W. Liu, L. Cui, W. Zhang, Y. Cao, *Pediatr. Res.* **2008**, *63*, 492.
[20] A. M. Smith, R. M. Shelton, Y. Perrie, J. J. Harris, *J. Biomater. Appl.* **2007**, *22*, 241.
[21] J. Sun, H. Tan, **2013**, *6*, 1285.
[22] S. M. Luna, M. E. Gomes, J. F. Mano, R. L. Reis, *J. Bioact. Compat. Polym.* **2010**, *25*, 341.
[23] S. J. Hollister, *Nat. Mater.* **2005**, *4*, 518.
[24] M. Fantini, M. Curto, F. De Crescenzio, *Virtual Phys. Prototyp.* **2016**, *11*, 77.
[25] Q. L. Loh, C. Choong, *Tissue Eng. Part B Rev.* **2013**, *19*, 485.
[26] S. Abdollahi, A. Davis, J. H. Miller, A. W. Feinberg, *PLoS One* **2018**, *13*, e0194890.
[27] T. J. Hinton, A. Hudson, K. Pusch, A. Lee, A. W. Feinberg, *ACS Biomater. Sci. Eng.* **2016**, *2*, 1781.
[28] E. S. Bishop, S. Mostafa, M. Pakvasa, H. H. Luu, M. J. Lee, J. M. Wolf, G. A. Ameer, T. C. He, R. R. Reid, *Genes Dis.* **2017**, *4*, 185.
[29] A. Blaeser, D. F. Duarte Campos, U. Puster, W. Richtering, M. M. Stevens, H. Fischer, *Adv. Healthcare Mater.* **2016**, *5*, 326.
[30] N. Paxton, W. Smolan, T. Böck, F. Melchels, J. Groll, T. Jungst, *Biofabrication* **2017**, *9*, 044107.
[31] R. A. Perez, M. Kim, T.-H. Kim, J.-H. Kim, J. H. Lee, J.-H. Park, J. C. Knowles, H.-W. Kim, *Tissue Eng., Part A* **2014**, *20*, 103.
[32] R. A. Perez, H. W. Kim, *Acta Biomater.* **2015**, *21*, 2.
[33] S. R. Caliari, J. A. Burdick, *Nat. Methods* **2016**, *13*, 405.
[34] A. Mishra, B. Starly, *Microfluid. Nanofluidics* **2009**, *6*, 373.
[35] S. P. Lyu, J. Schley, B. Loy, D. Lind, C. Hobot, R. Sparer, D. Untereker, *Biomacromolecules* **2007**, *8*, 2301.
[36] C. C. Dufort, M. J. Paszek, V. M. Weaver,. *Nat. Rev. Mol. Cell Biol.* **2011**, *12*, 308.
[37] T. R. Cox, J. T. Erler, *Dis. Models Mech.* **2011**, *4*, 165.
[38] L. Kass, J. T. Erler, M. Dembo, V. M. Weaver, *Int. J. Biochem. Cell Biol.* **2007**, *39*, 1987.